Int. J. Heat Mass Transfer. Vol. 25, No. 9, pp. 1321–1331, 1982
Printed in Great Britain

0017-9310/82/091321-11 $03.00/0
Pergamon Press Ltd.

THE EFFECT OF HEAT TRANSFER ON THREE-DIMENSIONAL SPATIAL STABILITY AND TRANSITION OF FLAT PLATE BOUNDARY LAYER AT MACH 3

A. R. WAZZAN and H. TAGHAVI
University of California, Los Angeles, U.S.A.

(*Received* 12 *March* 1982)

Abstract—The 3-dim. linear spatial stability of compressible flat plate boundary layers with heat transfer is investigated for the parallel flow assumption. The mean flow is obtained from the standard compressible boundary layer equations assuming perfect gas fluid properties, Sutherland's law of viscosity and constant Prandtl number.

Stability characteristics, amplification maps, are obtained for 2-dim. and 3-dim. modes at Mach 3.0 and ratio of wall to adiabatic wall temperature equal to 1.5, 1.25, 1.0, 0.8, 0.7 and 0.3. Results show that the stability of a given boundary layer cannot be concluded simply on the basis of the critical Reynolds number—incorrect conclusions may be made unless the entire instability map, particularly growth factors vs frequency and Reynolds number, is evaluated. Computations for the first 3-dim. mode show that, except for the 'transition reversal' the observed variation of the transition Reynolds number with heat transfer at the wall (cooling and heating) is predicted, qualitatively, by linear instability theory. Also, since the dominance of an instability mode can switch as major parameters affecting the disturbance are changed, transition reversal is predicted by the linear theory when with extended surface cooling the first 3-dim. mode, which is monotonically stabilized with cooling, ceases to be important and transition is then determined by the second 2-dim. mode.

NOMENCLATURE

A, local disturbance level;
A_0, initial disturbance amplitude, or level;
A_r, disturbance reference amplitude;
a, amplification factor defined in equation (11);
c, nondimensional wave speed of the disturbance;
C_p, specific heat at constant pressure;
f, transformed dimensionless stream function of the mean flow;
g, nondimensional enthalpy in the energy equation;
k, undisturbed thermal conductivity;
k', perturbed thermal conductivity;
$\bar{k}$, combined thermal conductivity, $\bar{k} = k + k'$;
K, λ/μ;
M, Mach number;
p, combined value of pressure, $p = P + p'$;
p', perturbation value of pressure;
P, undisturbed or mean value of pressure nondimensionalized by P_e;
Pr, Prandtl number, $C_p\mu/k$;
q, general amplitude function for the perturbation quantities;
q', general perturbation quantity;
R_A, Reynolds number corresponding to a given disturbance amplification ratio;
R_c, critical Reynolds number based on δ^*;
R_x, Reynolds number, $(\rho_e U_e x)/\mu_e$;
$\mathscr{R}$, universal gas constant;
Re_{δ^*}, Reynolds number, $(\rho_e U_e \delta^*)/\mu_e$;
Re, Reynolds number, $(\rho_e U_e \delta)/\mu_e$;
t, time [s] or nondimensionalized by δ/U_e;
T, undisturbed or mean temperature nondimensionalized by T_e;
T_0, stagnation temperature;
T_r, recovery temperature;
$\bar{T}$, combined mean and perturbed temperature, $\bar{T} = T + T'$;
T', perturbed value of temperature or dT/dy;
u, combined mean and perturbed velocity in x-direction, $u = U + u'$;
u', perturbed velocity in x-direction;
U, undisturbed velocity in x-direction nondimensionalized by U_e;
v, combined mean and perturbed velocity in y-direction, $v = V + v'$;
V, undisturbed velocity in the y-direction or nondimensionalized by U_e;
w, combined mean and perturbed velocity in z-direction, $w = W + w'$;
w', perturbed velocity in z-direction;
W, mean velocity in z-direction or nondimensionalized by U_e;
x, coordinate along the surface of the body or nondimensionalized by δ;
y, coordinate normal to the surface of the body [ft] or nondimensionalized by δ or general function in finite difference derivatives;
z, coordinate normal to the xy-plane.

Greek symbols

α_δ wavenumber of the disturbance along x-

axis nondimensionalized by δ;
β_δ, wavenumber of the disturbance along z-axis nondimensionalized by δ;
δ, boundary layer thickness at $U/U_e = 0.999$;
δ^*, displacement thickness;
η, transformed dimensionless coordinate normal to the surface;
η_δ, value of η at the outer edge of the boundary layer;
γ, ratio of specific heats, $\gamma = 1.4$ for air;
λ, undisturbed bulk viscosity;
λ', perturbed bulk viscosity;
$\bar{\lambda}$, $\bar{\lambda} = \lambda + \lambda'$;
μ, undisturbed or mean viscosity or nondimensionalized by μ_e;
μ', perturbed viscosity;
$\bar{\mu}$, combined mean and perturbed value of viscosity, $\bar{\mu} = \mu + \mu'$;
ν, kinematic viscosity;
ω, nondimensional frequency of the disturbance, a real number;
ψ, angle of the normal to the wave front and x-axis;
ρ, undisturbed density or nondimensionalized by ρ_e;
ρ', perturbation value of density;
$\bar{\rho}$, combined density, $\bar{\rho} = \rho + \rho'$.

Subscripts

A, adiabatic value;
c, critical;
e, value at the edge of boundary layer;
i, imaginary part;
n, neutral stability;
r, reference quantity or real part of a complex number;
x, based on x;
t, transition;
w, value at the wall or surface.

Superscripts

$'$, first derivative with respect to η or y;
$''$, second derivative with respect to η or y;
$\tilde{}$, indicates quantities transformed to a coordinate normal to the wave fronts.

INTRODUCTION

THE ROLE of Tollmien–Schlichting waves (TS mechanism) in the transition process of compressible laminar boundary layers has been the subject of many investigations. The effect of heating on the critical Reynolds number R_c was determined [1] in the Mach number range $0 \leqslant M \leqslant 3$; R_c decreased monotonically with heating. This trend was found parallel to the effect of heating on the transition Reynolds number R_t as measured [2] on a flat plate at $M \simeq 0.2$, on a cone at $M = 1.5$ and 2.0 [2], on a cone-cylinder at $M = 2.87$ [4] and on a flat plate at $M = 2.4$ [5]. Although the agreement in trend is good, R_c was of course orders of magnitude lower than R_t and the indicated effect of heating on R_c was much larger than its measured effect on R_t.

At moderate Mach numbers, moderate wall cooling for flat plates, cones and cone-cylinder leads to an increase in R_t [6–9]. However, with continued cooling the trend reverses and R_t decreases 'transition reversal'. Transition reversal was observed by Merlet and Rumsey [10] on 10° cones in supersonic free-flight tests. At $M \simeq 3$ the reversal occurred in the range $0.35 < T_w/T_r < 0.615$. Transition reversal was also observed on cones tested in the ballistic range at hypersonic Mach numbers [11]; at the higher values of M, the reversal was generally observed only at high unit Reynolds numbers. Van Driest and Boison [9] demonstrated that roughness cooperating with cooling may lead to transition reversal. This explanation, however, is not satisfactory with respect to transition reversal as may occur when extreme cooling is applied to smooth surfaces [12].

Mack [13], in a pioneering work on compressible boundary layer stability, through computer calculations, discovered new 2-dim. and skew modes that are more unstable than the first 2-dim. mode, which was considered in earlier studies, but they also exhibit the opposite response to cooling. So the dominance of a mode can switch as the major parameters affecting the disturbance are changed. Mack's calculations were later confirmed in microscopic experiments [14].

Mack's computation of R_c from the complete compressible stability equations, show that whereas the first 2-dim. mode is completely stabilized with extensive cooling, the second mode is destabilized. Therefore transition reversal contrasts with Mack's stability predictions for any one mode. Nevertheless, many comparisons of transition experiments and the corresponding stability theory indicate that in many cases of supersonic [6–9, 15–21] and some cases of hypersonic [22–36] transition, the TS mechanism may describe the substantial growth of disturbances before the emergence of the final 3-dim. turbulent spots and wedges.

Transition reversal on smooth surfaces has not been borne out yet by any of the compressible instability computations. For example, Lees and Reshotko's [27] compressible instability calculations which led to nonmonotonic stability trend with cooling, could possibly lead to transition reversal. However, the more recent calculations of Mack [28] based on the exact numerical solutions of the complete stability equations, exhibited monotonic trend with cooling. Doetsch [29], using Mack's stability equations, calculated the neutral curves for the first mode of 2-dim. disturbances on a flat plate ($M = 1.8$) at cooling ratios far in excess of those required for complete quenching of this mode in the hope of detecting a reversal but without success. This study however, should not be construed as complete evidence that stability theory fails to predict transition reversal on smooth surfaces with extended cooling—on occasions, the variation of the critical Reynolds number with a certain parameter contrasts

with the variation in other stability characteristics, such as the local amplification rates, e.g. with the same parameter [12].

An examination of available computations on the effect of cooling on stability characteristics suggest that transition reversal may be investigated through an examination of the effect of heat transfer on both the first and second modes rather than the first mode alone. For example, Mack's calculations at $M = 5.8$ reveal that whereas the first mode is quenched with cooling, the second mode becomes more amplified and shifts to higher frequencies. Reshotko and Stollery [30] suggested that the higher modes are ever present in hypersonic wind tunnels, while they are irrelevant in the ballistic range.

Yates and Donaldson [31] computed transition for Mach numbers between $M = 0$ and 12 at wall temperature ratios between 0.05 and 1.2. In the entire Mach number range they showed that (i) at constant wall temperature R_t increases monotonically with increasing M, (ii) at constant Mach number (any value) wall cooling decreases the transition Reynolds number (Fig. 4 of ref. [1]). Both results are not borne out by experiment. (It is commonly accepted that with increasing M, experiment shows R_t decreases from its value at $M = 0$, levels between about $M = 1.5$ and 4.0, then begins to increase again.)

More recently Mack [32] applied linear instability theory to the transition problem of flat plate (adiabatic and cooled) supersonic boundary layers. Amplification curves were computed for 2-dim. and skewed modes at several Mach numbers ($M = 1.3$–5.8). These growth curves were used in computing the transition Reynolds number R_A using the amplification-ratio criterion (e^n criterion) as proposed by Smith [33] for incompressible flows. Mack used several criterion: (i) the initial disturbance level A_0 is constant, (ii) A_0 is proportional to M^2, (iii) A_0 is proportional to M^2 and to the square root of the energy density of the 1-dim. power spectra of free stream disturbances as measured in supersonic wind tunnels. Whereas Smith found that in incompressible flows $(A/A_0) = e^9$ can be used as a criterion for transition, Mack selected, arbitrarily, the values of $(A/A_r) = 400$ or 100, where A_r is a reference amplitude. Calculations were made with $A_r = A_0$ and with $A_0 = A_r(M/1.3)^2$ when $M > 1.3$. Four curves were thus obtained. The Reynolds number R_A corresponding to these amplifications ratios were plotted as a function of M (Fig. 4 of ref. [32]). All curves showed a minimum near $M = 4.0$ and a maximum near $M = 2.0$; the magnitude of R_A at the minimum point differed from one curve to the other. Experiment does not verify (but neither does it positively rule out) the possibility of a maximum in R_t vs M at $M = 2.0$. On the other hand, Coles [34] measured the start of transition Reynolds number R_t on flat plates as a function of M; he found R_t shows a minimum near $M = 4.0$. Mack noted that agreement between the variation of R_t (measured), and R_A (computed) with M improved when A_0 was taken proportional to M^2 and to the square root of the energy density of the 1-dim. power spectra of the free stream disturbance, and when $(A/A_r) = 100$ or 50 (Fig. 5 of ref. [32]). In addition Mack computed the effect of wall cooling at $M = 3.0$ with assumptions (i) and (iii). The computed R_A was found to increase much more rapidly with cooling than observed experimentally (Fig. 9 of ref. [32]). However, when A_0 was determined from the forced response of the boundary layer to irradiated sound and from the measured free-stream power spectrum and arbitrarily choosing $(A/A_r) = 25 \doteq e^{3.25}$ a rise in R_A similar to what was observed by Van Driest and Blumer [35] was obtained (Fig. 9 of ref. [32]). These results were encouraging.

In the present paper the mean flow is computed by calculating the undisturbed compressible boundary layer equations using a 5-point finite difference scheme developed by Keltner [36]. The mean profiles are calculated using perfect gas fluid properties, Sutherland's law of viscosity and constant Prandtl number. The stability problem is approached by numerically solving the full 3-dim. compressible stability equations simultaneously. The finite difference technique of Keltner is used in the numerical solution, but for more accuracy 4 and 5, rather than 2 and 3, point Lagrangian derivatives are employed. Since transition experiments indicate that transition arises from the spatial rather than temporal, growth of disturbances, *all* the present calculations are done at $M = 3.0$ for *spatially* growing disturbances, within the framework of the quasi-parallel approximation.

ANALYSIS

The mean flow

The mean flow profiles are computed by solving the laminar heated and cooled compressible boundary layer equations in air using the method of Keltner [36]. Perfect fluid properties, Sutherland's law of viscosity, and constant Prandtl number are assumed.

Linearized spatial stability analysis

To derive the compressible stability equations a small 3-dim. disturbance (prime quantities) is added to the mean flow (non-primed quantities) such that

$$\begin{aligned} u &= U + u', \quad \bar{T} = T + T', \quad \bar{\mu} = \mu + \mu', \\ v &= V + v', \quad \bar{\rho} = \rho + \rho', \quad \bar{k} = k + k', \\ w &= W + w', \quad p = P + p', \quad \bar{\lambda} = \lambda + \lambda'. \end{aligned} \tag{1}$$

The stability equations are derived using the following assumptions:

(1) The mean flow satisfies the equations of motion.
(2) A small disturbance is imposed on the mean flow such that the nonlinear terms could be neglected.
(3) The mean flow is assumed to be parallel to the surface, i.e. $\partial/\partial x \ll \partial/\partial y$ (or there is no boundary layer growth).
(4) Perfect gas fluid properties with Sutherland's

law of viscosity are assumed and Pr and C_p are taken to be constants.

To obtain the perturbation equations, the combined flow components are substituted into the equations of motion. Subsequently, the mean flow equations of motion are subtracted from the combined flow equations and the nonlinear and nonparallel mean flow terms are dropped. This results in a set of five linear equations in u', v', w', T', p', with ρ' obtained from the equation of state. Oblique disturbances are considered; the mean flow makes an angle ψ with the normal to the wave front. To simplify the stability equations, the coordinate system, following Mack [28, 32], is rotated to coincide with that of the wave front. The resulting coordinate system is designated the 'tilde' coordinate system. Following the procedure outlined above the following set of perturbation (disturbance) equations is obtained:

$$\frac{\partial \rho'}{\partial t} + \rho\left(\frac{\partial \tilde{u}'}{\partial \tilde{x}} + \frac{\partial \tilde{v}'}{\partial y}\right) + \tilde{U}\frac{\partial \rho'}{\partial x} + \tilde{v}'\frac{\partial \rho}{\partial y} = 0, \tag{2}$$

$$\begin{aligned}\rho\left(\frac{\partial \tilde{u}'}{\partial \tilde{t}} + \tilde{u}\frac{\partial \tilde{u}'}{\partial \tilde{x}} + \tilde{v}'\frac{\mathrm{d}\tilde{U}}{\mathrm{d}y}\right) - \tan\psi\left[\rho\left(\frac{\partial \tilde{w}}{\partial \tilde{t}} + \tilde{u}\frac{\partial \tilde{w}}{\partial \tilde{x}} + \tilde{v}'\frac{\mathrm{d}\tilde{W}}{\mathrm{d}y}\right)\right] \\ = -\frac{1}{\gamma \tilde{M}_e^2}\frac{\partial p'}{\partial \tilde{x}'} + \frac{1}{\tilde{Re}_\delta}\left\{2\mu\cos^2\psi\left(\frac{\partial^2 \tilde{u}'}{\partial \tilde{x}^2} - \frac{\partial^2 \tilde{w}'}{\partial \tilde{x}^2}\tan\psi\right) + \frac{2}{3}(\lambda - \mu)\right. \\ \times\left(\frac{\partial^2 \tilde{u}'}{\partial \tilde{x}^2} + \frac{\partial^2 \tilde{v}'}{\partial \tilde{x}\partial y}\right) + \mu\left[2\frac{\partial^2 \tilde{u}'}{\partial \tilde{x}^2}\sin^2\psi + \frac{\partial^2 \tilde{u}'}{\partial y^2} + \frac{\partial^2 \tilde{v}'}{\partial \tilde{x}\partial y} + \frac{\partial^2 \tilde{w}'}{\partial \tilde{x}^2}\right. \\ \times(2\cos^2\psi - 1)\tan\psi - \left.\frac{\partial^2 \tilde{w}'}{\partial y^2}\tan\psi\right] + \frac{\mathrm{d}\mu}{\mathrm{d}y}\left(\frac{\partial \tilde{u}'}{\partial y} + \frac{\partial \tilde{v}'}{\partial \tilde{x}} - \frac{\partial \tilde{w}'}{\partial y}\tan\psi\right) \\ \left. + \mu'\left(\frac{\mathrm{d}^2\tilde{U}}{\mathrm{d}y^2} - \frac{\mathrm{d}^2\tilde{W}}{\mathrm{d}y^2}\tan\psi\right) + \frac{\partial \tilde{\mu}'}{\partial y}\left(\frac{\mathrm{d}\tilde{U}}{\mathrm{d}y} - \frac{\mathrm{d}\tilde{W}}{\mathrm{d}y}\tan\psi\right)\right\},\end{aligned} \tag{3}$$

$$\begin{aligned}\rho\left(\frac{\partial \tilde{v}'}{\partial t} + \tilde{U}\frac{\partial \tilde{v}'}{\partial \tilde{x}}\right) = -\frac{1}{\gamma \tilde{M}_e^2}\frac{\partial p'}{\partial y} + \frac{1}{\tilde{Re}_\delta}\left[2\mu\frac{\partial^2 \tilde{v}'}{\partial y^2} + \frac{2}{3}(\lambda - \mu)\right. \\ \times\left(\frac{\partial^2 \tilde{u}'}{\partial \tilde{x}\partial y} + \frac{\partial^2 \tilde{v}'}{\partial y^2}\right) + \mu\left(\frac{\partial^2 \tilde{u}'}{\partial \tilde{x}\partial y} + \frac{\partial^2 \tilde{v}'}{\partial \tilde{x}^2}\right) + 2\frac{\mathrm{d}\mu}{\mathrm{d}y}\frac{\partial \tilde{v}'}{\partial y} \\ \left. + \frac{\partial \mu'}{\partial \tilde{x}}\frac{\mathrm{d}\tilde{U}}{\mathrm{d}y} + \frac{2}{3}\left(\frac{\mathrm{d}\lambda}{\mathrm{d}y} - \frac{\mathrm{d}\mu}{\mathrm{d}y}\right)\left(\frac{\partial \tilde{u}'}{\partial \tilde{x}} + \frac{\partial \tilde{v}'}{\partial y}\right)\right],\end{aligned} \tag{4}$$

$$\begin{aligned}\rho\left(\frac{\partial \tilde{w}'}{\partial \tilde{t}} + \tilde{v}'\frac{\mathrm{d}\tilde{W}}{\mathrm{d}y} + \tilde{U}\frac{\partial \tilde{w}'}{\partial \tilde{x}}\right) + \tan\psi\left[\rho\left(\frac{\partial \tilde{u}'}{\partial \tilde{t}} + \tilde{U}\frac{\partial \tilde{u}'}{\partial \tilde{x}} + \tilde{v}'\frac{\mathrm{d}\tilde{U}}{\mathrm{d}y}\right)\right] \\ = -\frac{1}{\gamma \tilde{M}_e^2}\frac{\partial p'}{\partial \tilde{x}}\tan\psi + \frac{1}{\tilde{Re}_\delta}\left\{2\mu\sin^2\psi\left(\frac{\partial \tilde{u}'}{\partial \tilde{x}^2}\tan\psi + \frac{\partial^2 \tilde{w}'}{\partial \tilde{x}^2}\right)\right. \\ + \frac{2}{3}(\lambda - \mu)\left[\tan\psi\left(\frac{\partial^2 \tilde{u}'}{\partial \tilde{x}^2} + \frac{\partial^2 \tilde{v}'}{\partial \tilde{x}\partial y}\right)\right] + \mu\left[2\cos^2\psi\tan\psi\frac{\partial^2 \tilde{u}'}{\partial \tilde{x}^2}\right. \\ \left. + (2\cos^2\psi - 1)\frac{\partial^2 \tilde{w}'}{\partial \tilde{x}^2} + \tan\psi\frac{\partial^2 \tilde{v}'}{\partial \tilde{x}\partial y} + \tan\psi\frac{\partial^2 \tilde{u}'}{\partial y^2} + \frac{\partial^2 \tilde{w}'}{\partial y^2}\right] \\ + \frac{\mathrm{d}\mu}{\mathrm{d}y}\left[\frac{\partial \tilde{w}'}{\partial y} + \tan\psi\left(\frac{\partial \tilde{u}'}{\partial y} + \frac{\partial \tilde{v}'}{\partial \tilde{x}}\right)\right] + \mu'\left(\frac{\mathrm{d}^2\tilde{U}}{\mathrm{d}y^2}\tan\psi + \frac{\mathrm{d}^2\tilde{W}}{\mathrm{d}y^2}\right) \\ \left. + \frac{\partial \mu'}{\partial y}\left(\frac{\mathrm{d}\tilde{U}}{\mathrm{d}y}\tan\psi + \frac{\mathrm{d}\tilde{W}}{\mathrm{d}y}\right)\right\},\end{aligned} \tag{5}$$

$$\begin{aligned}\rho\left(\frac{\partial T'}{\partial \tilde{t}} + \tilde{U}\frac{\partial T'}{\partial \tilde{x}} + \tilde{v}'\frac{\mathrm{d}T}{\mathrm{d}y}\right) = -(\gamma - 1)\left(\frac{\partial \tilde{u}'}{\partial \tilde{x}} + \frac{\partial \tilde{v}'}{\partial y}\right) \\ + \frac{\gamma}{Pr\tilde{Re}_\delta}\left[\mu\left(\frac{\partial^2 T'}{\partial \tilde{x}^2} + \frac{\partial^2 T'}{\partial y^2}\right) + \frac{\mathrm{d}\mu}{\mathrm{d}y}\frac{\partial T'}{\partial y} + \mu'\frac{\mathrm{d}^2 T}{\mathrm{d}y^2} + \frac{\partial \mu'}{\partial y}\frac{\mathrm{d}T}{\mathrm{d}y}\right] \\ + \frac{\gamma(\gamma - 1)\tilde{M}_e^2}{\tilde{Re}_\delta}\left\{2\mu\frac{\mathrm{d}\tilde{u}}{\mathrm{d}y}\left(\frac{\partial \tilde{u}'}{\partial y} + \frac{\partial \tilde{v}'}{\partial \tilde{x}}\right) + 2\mu\frac{\mathrm{d}\tilde{W}}{\mathrm{d}y}\frac{\partial \tilde{w}'}{\partial y}\right. \\ \left. + \mu'\left[\left(\frac{\mathrm{d}\tilde{U}}{\mathrm{d}y}\right)^2 + \left(\frac{\mathrm{d}\tilde{W}}{\mathrm{d}y}\right)^2\right]\right\},\end{aligned} \tag{6}$$

$$p' = \rho' T + \rho T'. \tag{7}$$

Then, [equation (3) + $\tan\psi$ equation (5)] yields

$$\rho\left(\frac{\partial \tilde{u}'}{\partial \tilde{t}} + \tilde{U}\frac{\partial \tilde{u}'}{\partial \tilde{x}} + \tilde{v}'\frac{d\tilde{U}}{dy}\right) = -\frac{1}{\gamma \tilde{M}_e^2}\frac{\partial p'}{\partial \tilde{x}} + \frac{1}{\tilde{R}e_\delta} \times \left[2\mu\frac{\partial^2 \tilde{u}'}{\partial \tilde{x}^2} + \frac{2}{3}(\lambda - \mu)\left(\frac{\partial^2 \tilde{u}'}{\partial \tilde{x}^2} + \frac{\partial^2 \tilde{v}'}{\partial \tilde{x}\partial y}\right) + \mu\left(\frac{\partial^2 \tilde{u}'}{\partial y^2} + \frac{\partial^2 \tilde{v}'}{\partial \tilde{x}\partial y}\right) + \frac{d\mu}{dy}\left(\frac{\partial \tilde{u}'}{\partial y} + \frac{\partial \tilde{v}'}{\partial \tilde{x}}\right) + \mu'\frac{d^2\tilde{U}'}{dy^2} + \frac{\partial \mu'}{\partial y}\frac{d\tilde{U}}{dy}\right] \tag{8}$$

and, [equation (5) − $\tan\psi$ equation (3)] yields

$$\rho\left(\frac{\partial \tilde{w}'}{\partial \tilde{t}} + \tilde{v}'\frac{d\tilde{W}}{dy} + \tilde{U}\frac{\partial \tilde{w}'}{\partial \tilde{x}}\right) = \frac{1}{\tilde{R}e_\delta}\left[\mu\left(\frac{\partial^2 \tilde{w}'}{\partial \tilde{x}^2} + \frac{\partial^2 \tilde{w}'}{\partial y^2}\right) + \frac{d\mu}{dy}\frac{\partial \tilde{w}'}{\partial y} + \mu'\frac{d^2\tilde{W}}{dy^2} + \frac{\partial \mu'}{\partial y}\frac{d\tilde{W}}{dy}\right] \tag{9}$$

so with $\partial/\partial\tilde{z} = 0$, all $\tilde{w}'$ and W terms drop out of the $\tilde{x}$ and y momentum and continuity equations.

The disturbance quantities are now written in a wave-type form:

$$\tilde{q}'(\tilde{x}, y, \tilde{z}, t) = \tilde{q}(y)e^{i(\tilde{\alpha}_\delta \tilde{x} + \tilde{\beta}_\delta \tilde{z} - \tilde{\alpha}_\delta c t)} \tag{10}$$

with $\tilde{\alpha}_\delta$ the wave number taken to be a complex number, c the dimensionless wave speed is complex and $\tilde{\omega} = \tilde{\alpha}_\delta c/\tilde{R}_\delta = \omega/\cos^2\psi$ is the dimensionless frequency and is taken to be real (spatial growth). The resulting stability equations are solved simultaneously using a 4 and 5 point finite difference and matrix triangularization technique.

RESULTS AND DISCUSSION

In compressible flow there are infinite number of instability modes. According to Mack [28, 32] higher modes become important only at high Mach numbers. Mack did not, for example, find higher modes below $M = 3.8$. In the present calculations higher modes are found at $M = 3.0$. The higher modes are frequently more unstable than the first mode, especially at high Mach numbers. Two reasons account for this. First, the viscous terms have less effect for higher modes. Equations (2)–(10) show that the viscous terms are multiplied by $1/\alpha_\delta R_\delta$. Therefore, the higher modes would be expected to assume more and more inviscid instability characteristics. Second, due to the density variation across the boundary layer at high Mach numbers, the inviscid terms themselves become more important. These two effects combine to make the higher modes assume more inviscid instability characteristics. The inviscid characteristics or the higher modes may provide an answer to the phenomenon of transition reversal in compressible layers. Cooling affects the stability of the boundary layer through the viscous terms and quenches the unstable regions. That is, with cooling the lower modes are quenched and higher and higher modes, which assume more and more inviscid character, come into play. In turn, these more and more inviscidly behaving modes become less and less affected by cooling, and the trend to increased stability with surface cooling is reduced. Hence, it is possible that the effect of cooling on a high mode, say at ratio of wall to adiabatic wall temperature $T_w/T_{A_w} = 0.2$, is less than its effect at $T_w/T_{A_w} = 0.8$. This behavior can lead to the transition reversal observed with extended cooling. This possibility is explored in a later section of this paper.

For incompressible flow Squire [37] proved that 2-dim. disturbances are more unstable than 3-dim. disturbances. This follows from the fact that the stability equations for oblique waves are *identical* to the ones for 2-dim. waves; therefore, oblique waves have higher R_c than 2-dim. waves. Thus it would be necessary to only consider 2-dim. waves. In compressible flow, however, the stability equations for 2-dim. and oblique disturbances are different [28, 38]. The oblique energy equation (6) contains in the viscous dissipation terms, a term involving $\tilde{w}'$ which does not vanish and cannot be ignored. The result, therefore is, that the 3-dim. oblique waves are more unstable than the 2-dim. waves [28, 38]. Therefore, in studying transition the most unstable oblique waves (i.e. ψ_{max}) must be determined. Fortunately, computations [28, 38] show that the *most unstable 3-dim. mode is the first mode*; the second and higher 3-dim. modes become quickly stable with a slight change of angle ψ from the normal. Also, sensitivity studies showed it is adequate to use 4 and 5 point Lagrangian derivatives and 200 point computations across the boundary, in solving the 3-dim. compressible stability equations.

Computations, like the one shown in Fig. 1, show that for the first 3-dim. mode at $M = 3.0$ the most dangerous wave angle is $\psi = 60°$. Therefore, complete stability calculations at $M = 3.0$ were made at $\psi = 60°$. Figure 1 indicates that, as expected, the first 3-dim. mode is much more unstable than the first 2-dim. mode ($\psi = 0°$). Figure 2 is the stability map of constant spatial amplification rates on the ω vs R_{δ^*} diagram for the first 3-dim. mode at the most dangerous wave angle

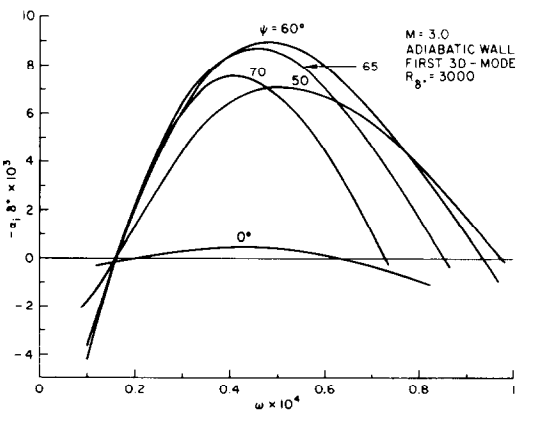

FIG. 1. Amplification rates vs frequency.

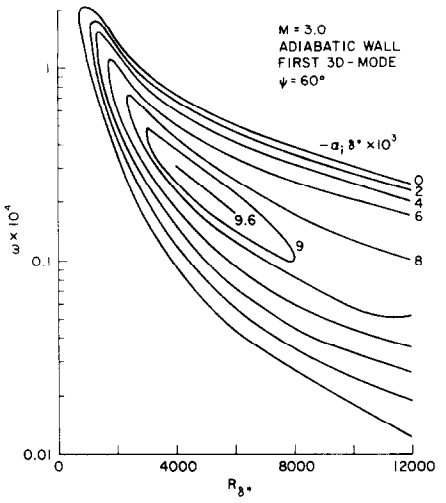

FIG. 2. Curves of constant amplification rates.

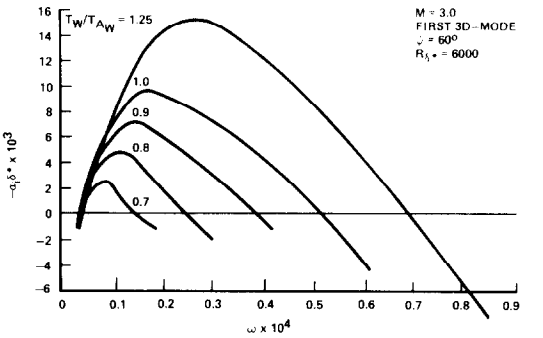

FIG. 3. Effects of heating and cooling on amplification rates.

ψ; the neutral curve corresponds to $\alpha_i\delta^* = 0$. The maximum amplification rate $\alpha_i\delta^*$ of -9.6×10^{-3} is about 20 times the value obtained by Keltner for the first 2-dim. mode [36].

To investigate the effect of heating and cooling on the stability parameters and the transition Reynolds number for flat plate at $M = 3.0$, a number of cases were calculated for $T_w/T_{A_w} = 1.5$–0.7. Some boundary layer parameters are listed in Table 1.

Table 1 shows that U''_w increases with heating and becomes more negative with cooling. Incompressible studies [39] show that stability is increased as U''_w decreases. Figure 3, a plot of amplification rates vs frequency for different values of T_w/T_{A_w}, shows that this is true for the first 3-dim. mode in compressible flow. Figure 3 shows that wall cooling, at $M = 3.0$, $R_{\delta^*} = 6000$ and $\psi = 60°$, damps the first 3-dim. mode; in fact, at $R_{\delta^*} = 6000$ and $T_w/T_{A_w} = 0.6$, the first 3-dim. mode is completely damped.

Stability computations at $T_w/T_{A_w} = 0.8$ showed that, as in the case of adiabatic wall, the most dangerous disturbances still are at $\psi \doteq 60°$. Therefore *all* of the calculations for heat transfer at the wall were done at $\psi = 60°$. The stability maps for these cases are shown in Figs. 4–7. The neutral curve for $T_w/T_{A_w} = 0.6$ was also calculated; the critical Reynolds number is found at $R_c = 8000$, but the amplification rates were too small to be of any consequence. Figures 4–7 and 2 show a monotonic increase in R_c with cooling and a decrease with heating. Also there is an increase of one order of magnitude in $(-\alpha_i\delta^*)_{max}$ as T_w/T_{A_w} increases from 0.7 to 1.5. It is also observed that the peak of the amplified frequency range decreases from about $\omega = 6 \times 10^{-4}$ at $T_w/T_{A_w} = 1.5$ to about $\omega = 0.6 \times 10^{-4}$ at $T_w/T_{A_w} = 0.7$; the range of amplified frequency, bounded by the neutral curve, is also substantially decreased. This indicates that, as expected, the boundary layer is destabilized with surface heating, but is stabilized with cooling.

The amplification rates were integrated with respect to R_{δ^*} along lines of constant frequency, and the growth curves obtained for each case; as examples Figs. 8 and 9 give the amplification ratios ln a vs R_x curves for $T_w/T_{A_w} = 1.5$ and 0.7. Transition Reynolds numbers would be predicted from the envelopes of

Table 1. Boundary layer values vs T_w/T_{A_w} at $M = 3.0$

T_w/T_{A_w}	f''_w	g_w	g'_w	η_δ	δ/δ^*	$R_{\delta^*}/R_x^{1/2}$
0.2	0.4571	0.1785	0.2883	4.254	3.414	1.78
0.3	0.4615	0.2678	0.2548	4.244	2.896	2.26
0.7	0.4814	0.6249	0.1140	4.204	2.033	4.12
0.8	0.4886	0.7142	0.0771	4.191	1.931	4.56
0.9	0.4962	0.8035	0.0391	4.178	1.849	5.01
1.0	0.5041	0.8928	0	4.165	1.781	5.43
1.25	0.5239	1.116	−0.1036	4.133	1.653	6.48
1.5	0.5431	1.339	−0.2150	4.102	1.564	7.50
T_w/T_{A_w}	U'_w	U''_w	T_w	T'_w	T''_w	μ_w
0.2	3.908	−51.82	0.5011	6.917	−129.9	0.4712
0.3	2.838	−15.83	0.7516	4.397	−44.8	0.7431
0.7	1.628	−0.8691	1.754	1.082	−7.276	1.690
0.8	1.521	−0.4270	2.004	0.6744	−6.040	1.894
0.9	1.440	−0.1645	2.255	0.3192	−5.283	2.087
1.0	1.377	0	2.505	0	−4.780	2.271
1.25	1.266	0.2126	3.132	−0.7032	−4.174	2.695
1.5	1.195	0.3018	3.758	−1.328	−3.947	3.078

these curves; $R_{x_i} = R_x$ evaluated at $\ln a$ equal to a given value, e.g. $\ln a \doteq 3.0$ where $\ln a$ is given by

$$\ln a = -\frac{2}{(R_{\delta^*}/\sqrt{R_x})^2}\int_{R_{\delta^*_n}}^{R_{\delta^*}} \alpha_i \delta^* \mathrm{d}R_{\delta^*}. \quad (11)$$

The transition measurements of Jack and Diaconis [7] and Diaconis *et al.* [8] on a 9.5° cone at a before-the-shock Mach number of $M = 3.12$, which corresponds to $M_e = 2.98$ after the shock, are shown in Fig. 10. The transition Reynolds number in these experiments was determined for conditions of heating and cooling at many values of unit Reynolds number and stagnation temperature T_0; these are listed in Fig. 10. Transition reversal was detected at $T_w/T_{A_w} = 0.25$. The computed transition Reynolds numbers are shown in Fig. 10 using amplification ratios of $e^{1.25}$, $e^{2.5}$ and $e^{3.0}$. It is seen that generally speaking, the effect of surface heat transfer on transition is predicted, qualitatively, by the theory. But, in all cases the computations show faster stabilization with cooling than the experiment does. Also, transition reversal is not predicted, even qualitatively, from the first 3-dim. mode stability computations.

To investigate the possibility of the higher modes, e.g. the second mode (2-dim. and/or 3-dim.) causing the transition reversal (see earlier in this section) requires eigenvalues for the second modes at $M = 3.0$. However, since the second 2-dim. mode is found to be the most unstable second mode [28, 38], calculations were done only with $\psi = 0°$. The second 2-dim. mode

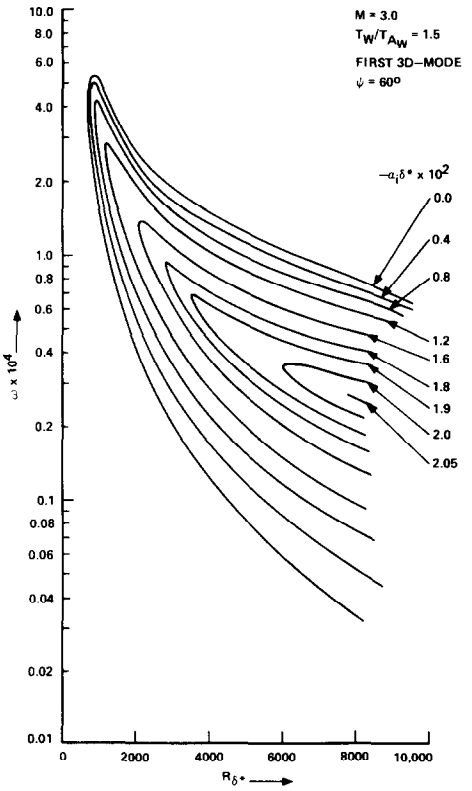

FIG. 4. Curves of constant amplification rates.

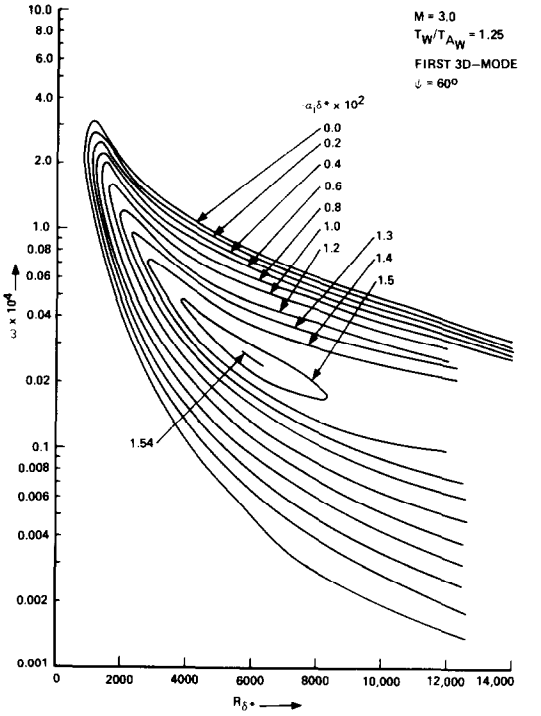

FIG. 5. Curves of constant amplification rates.

with adiabatic wall is found at higher frequencies than the first mode (Fig. 11). Its amplification rates are shown in Fig. 12. The maximum amplification rate for the second 2-dim. mode ($\alpha_i\delta^* = -120 \times 10^{-3}$) is more than two orders of magnitude larger than the first 2-dim. mode (-0.462×10^{-3}) and one order or magnitude larger than the first 3-dim. mode (-9.6×10^{-3}).

Figure 13 shows that with extended cooling the unstable region has moved to lower frequency. Also, the maximum amplification rate for the second 2-dim. mode at $R_{\delta^*} = 2000$ is decreased monotonically and substantially, indicating stabilization of the second 2-dim. mode with cooling. The latter conclusion is not

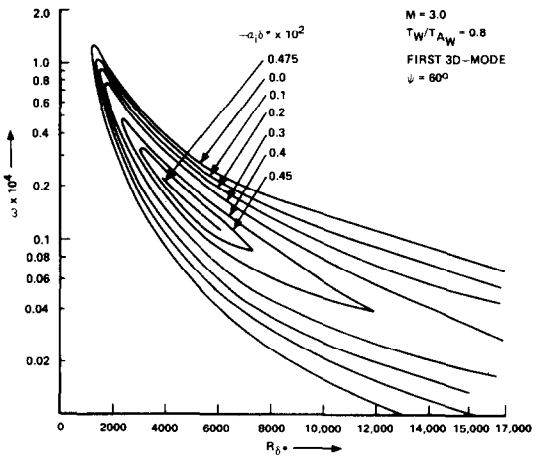

FIG. 6. Curves of constant amplification rates.

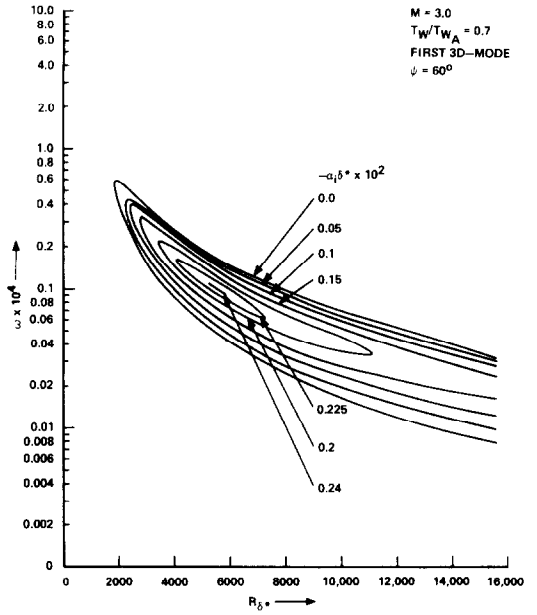

FIG. 7. Curves of constant amplification rates.

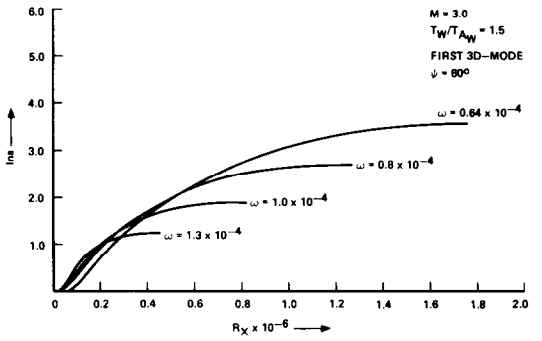

FIG. 8. Growth factor (a) at constant frequency vs Reynolds number, R_x.

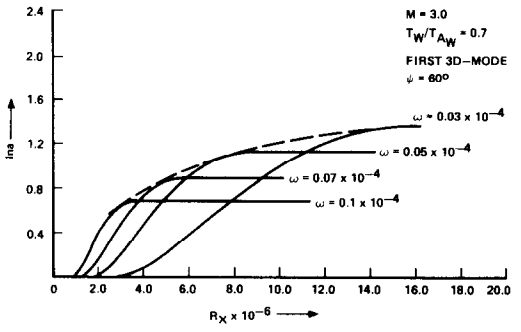

FIG. 9. Growth factor (a) at constant frequency vs Reynolds number, R_x.

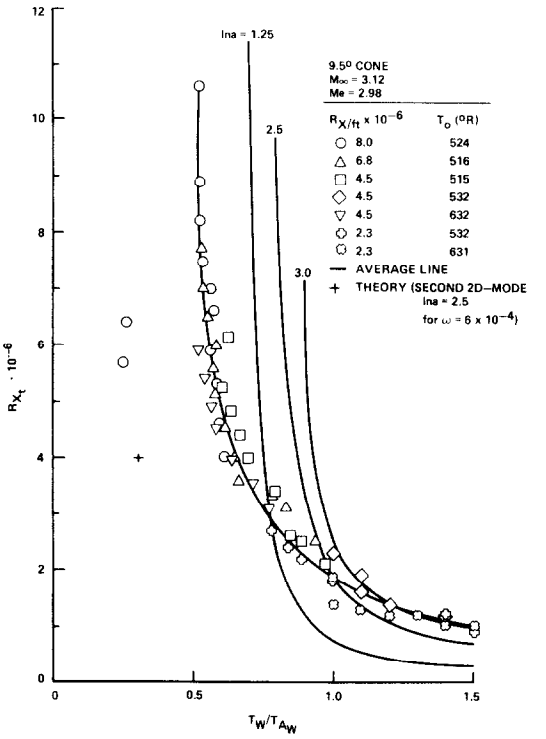

FIG. 10. Transition Reynolds number vs T_w/T_{A_w} at $M = 3$. Data after refs. [7, 8].

correct however. Further calculations at $T_w/T_{A_w} = 0.3$ showed (Figs. 11 and 14) that the unstable regions have moved to *smaller* Reynolds numbers, a destabilizing effect. Figure 14, for $\omega = 80 \times 10^{-4}$, shows the maximum amplification $(-\alpha_i\delta^*)_{max}$ rate, for this highly cooled case, at $R_{\delta^*} = 365$ is equal to 52×10^{-2} which is about 5 times larger than its value for the adiabatic case, 11×10^{-2} (Fig. 12) (Figure 14 also shows the existence of the third 2-dim. mode at these small Reynolds numbers. However, the third 2-dim. mode is ignored for the calculations of the growth

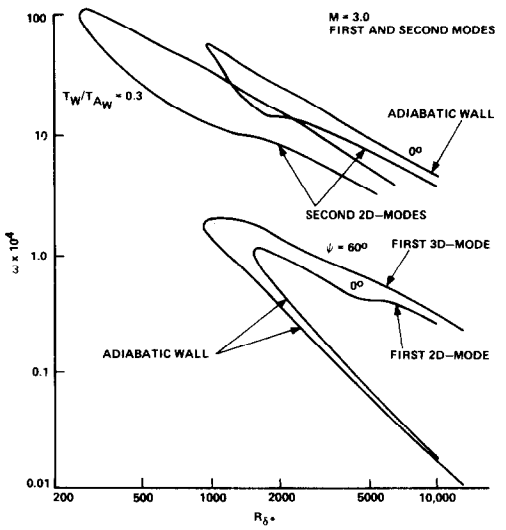

FIG. 11. Neutral curves for $M = 3$.

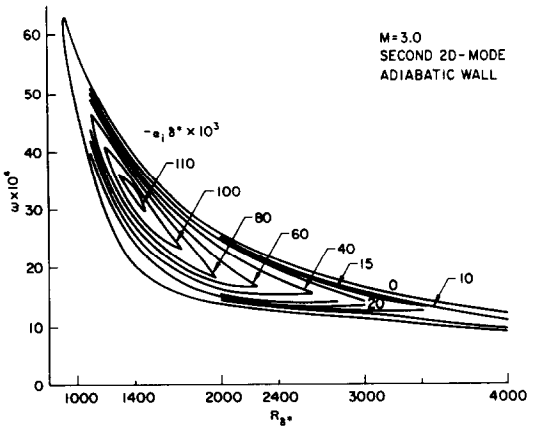

FIG. 12. Curves of constant amplification rates.

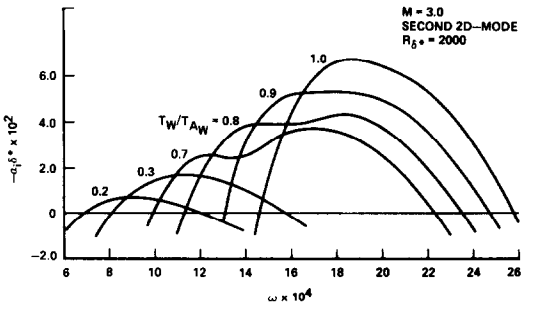

FIG. 13. Effect of cooling on amplification rates.

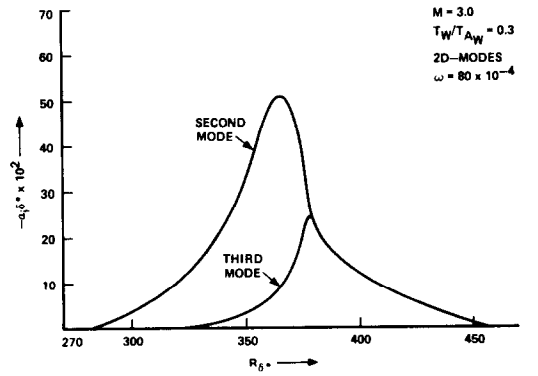

FIG. 14. Amplification rates vs Reynolds number R_{δ^*}.

factors since the third mode is seen to be more stable than the second 2-dim. mode.) Figure 11 gives a more complete picture of this behavior. For the adiabatic case, the first 3-dim. mode is less stable, smaller critical Reynolds number and larger unstable frequency range, than the first 2-dim. mode. It shows also the second 2-dim. mode gives almost the same critical Reynolds number as the first 3-dim. mode, but its unstable frequency range is smaller, although it occurs at higher frequencies. We also find that for the cooled case ($T_w/T_{A_w} = 0.3$) $R_c = 300$ which is below the adiabatic value of 980.

The transition data of Fig. 10 shows that with wall

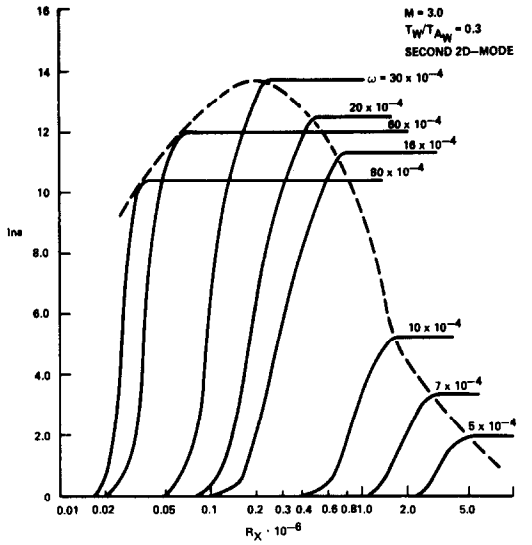

FIG. 15. Amplification factor (a) at constant frequency vs Reynolds number, R_x.

cooling the transition Reynolds number increases from about $R_{x_t} \doteq 10^6$ at $T_w/T_{A_w} = 1.5$ to about 11×10^6 at $T_w/T_{A_w} \doteq 0.5$, then drops to about 6×10^6 at $T_w/T_{A_w} \doteq 0.27$; this latter behavior is known as the transition reversal. Because of these and the results for the second 2-dim. versus the first 3-dim. mode we return to the second 2-dim. mode to determine if it can lead to stability (or transition) reversal. The growth factor curves ln a vs R_x were computed for the second 2-dim. mode at $T_w/T_{A_w} \doteq 0.3$ and are given in Fig. 15. This figure shows that for a growth factor of about ln $a \doteq 3.0$ a transition Reynolds number $\doteq 4 \times 10^6$ is predicted at $\omega \doteq 6 \times 10^{-4}$. [Note that this figure gives also a value of ln $a = 3.0$ at $R_x \doteq 0.015 \times 10^6$ and $\omega = 120 \times 10^{-4}$. However, we have selected the results that occur at the much lower frequency because the higher frequencies, $\omega \gg 10^{-4}$, may not occur in practice. Also note that for the 3-dim. mode (Figs. 4–7) the frequency range of interest is for $\omega \leq 10^{-4}$.] This value of $R_{x_t} = 4.0 \times 10^6$ is plotted in Fig. 10. It shows that with extended cooling, stability determination shifts from the first 3-dim. mode, which is strongly damped, to the second 2-dim. mode, as discussed above, and stability reversal with extended cooling is predicted, qualitatively, from linear theory.

SUMMARY AND CONCLUSIONS

The linear stability of heated and cooled compressible flat plate boundary layer is determined at $M = 3.0$; characteristics of 3-dim. and 2-dim. instability modes are determined. The first 3-dim. mode is found to be monotonically stabilized with wall cooling. The second 2-dim. mode, depending on the Reynolds number and frequency range, can exhibit both stabilization and destabilization with cooling. Except for regions of extended wall cooling where transition data exhibit transition reversal, the variation of the com-

puted transition Reynolds number with wall cooling is qualitatively similar to that exhibited by the transition data. Transition reversal can be predicted by linear theory as the instability mechanism shifts from the first 3-dim. to the second 2-dim. mode with cooling.

REFERENCES

1. E. R. Van Driest, Calculation of the stability of the laminar boundary layer in a compressible fluid on a flat plate with heat transfer, *J. Aero. Sci.* **19,** 801 (1952).
2. H. W. Liepmann and G. H. Fila, Investigation of effects of surface temperature and single roughness elements on boundary-layer transition, NACA TN No. 1196 (1947).
3. R. Scherrer, Boundary-layer transition on a cooled 20° cone at Mach numbers of 1.5 and 2.0, NACA TN No. 2131 (1950).
4. G. R. Eber, Recent investigations of temperature recovery and heat transmission on cones and cylinders in axial flow in the N.O.L. aeroballistics wind tunnel, *J. Aero. Sci.* **19,** 1 (1952).
5. W. Higgins and C. C. Pappas, An experimental investigation of the effect of surface heating on boundary layer transition on a flat plate in supersonic flow, NACA TN No. 2351 (1951).
6. R. Scherrer, Comparison of theoretical and experimental heat-transfer characteristics of bodies of revolution at supersonic speeds, NACA Tech. Rept. No. 1055 (1951).
7. J. R. Jack and N. S. Diaconis, Variation of boundary-layer transition with heat transfer on two bodies of revolution at a Mach number of 3.12, NACA TN 3562 (1955).
8. N. S. Diaconis, J. R. Jack and R. J. Wisniewski, Boundary-layer transitions at Mach 3.12 as affected by cooling and nose blunting, NACA TN 3928 (1957).
9. E. R. Van Driest and J. Ch. Boison, Experiments in boundary-layer transition at supersonic speeds, *J. Aero. Sci.* **24,** 885 (1957).
10. C. E. Merlet and C. B. Rumsey, Supersonic free-flight measurement of heat transfer and transition on a 10° cone having a low temperature ratio, NASA TN D-951 (1961).
11. N. W. Sheetz, Jr., Boundary-layer transition on cones at hypersonic speeds, in *Proc. Navy-NASA-LTV Symposium on Viscous Drag Reduction* (edited by J. D. Spangler and C. S. Wells, Jr.). Plenum Press (1969).
12. M. V. Morkovin, Critical evaluation of transition from laminar to turbulent shear layers with emphasis on hypersonically traveling bodies, U.S. AFFDL TR-68-149 (1969).
13. L. M. Mack, Stability of the compressible layer according to a direct numerical solution, AGARDograph 97, Part I, p. 329 (1965).
14. J. M. Kendall, Supersonic boundary layer stability experiments, Jet Propulsion Laboratory, Space Programs Summary 37–39, (1966).
15. D. W. Dunn and C. C. Lin, On the stability of the laminar boundary layer in a compressible fluid, *J. Aero. Sci.* **22,** 469 (1955).
16. M. Lessen, J. A. Fox and H. M. Zien, On the inviscid stability of the laminar mixing of two parallel streams of a compressible fluid, *J. Fluid Mech.* **23,** 355 (1965).
17. M. Lessen, J. A. Fox and H. M. Zien, Stability of the laminar mixing of two parallel streams with respect to supersonic disturbances, *J. Fluid Mech.* **25,** 737 (1966).
18. H. G. Gropengiesser, Ein Beitrag zur stabilität freier Grenzschichten in kimpressiblen Medien, Doctoral thesis, Hermann-Föttinger Institut für Strömungstechnik, Technische Universität Berlin (1968).
19. D. R. Chapman, D. M. Kuehn and H. K. Larson, Investigation of separated flows in supersonic and subsonic streams with emphasis on the effect of transition, NACA Tech. Rept. No. 1356 (1958).
20. H. K. Larson, Heat transfer in separated flows, *J. Aero. Sci.* **26,** 731 (1959).
21. H. K. Larson and S. J. Keating, Jr., Transition Reynolds numbers of separated flows at supersonic speeds, NASA TN D-349 (1960).
22. B. E. Richards and J. L. Stollery, Further experiments on transition reversal at hypersonic speeds, *AIAA J.* **4,** 2224 (1966).
23. R. E. Deem and J. S. Murphy, Flat plate boundary layer transition at hypersonic speeds, AIAA Paper No. 65-128 (1965).
24. R. J. Sanator, J. P. DeCarlo and D. T. Torrillo, Hypersonic boundary layer transition data for cold wall slender cone, *AIAA J.* **3,** 738 (1965).
25. N. W. Sheetz, Free-flight boundary layer transition investigations at hypersonic speeds, AIAA Paper No. 65-127 (1965).
26. B. E. Richards and J. L. Stollery, Transition reversal on a flat plate at hypersonic speeds, AGARDograph 97, p. 483 (1965).
27. L. Lees and E. Reshotko, Stability of the compressible laminar boundary layer, *J. Fluid Mech.* **12,** 555 (1962).
28. L. M. Mack, Notes on the theory of instability of incompressible and compressible laminar boundary layers, Von Karman Institute for Fluid Dynamics, Brussels, Belgium (1968).
29. K. H. Doetsch, unpublished thesis, Dept. of Aeronautics, Imperial College, London (1968).
30. E. Reshotko and J. L. Stollery, Further experiments on transition reversal at hypersonic speeds, *AIAA J.* **4,** 2224 (1966).
31. J. E. Yates and C. duP. Donaldson, Transition run-out calculations for a compressible boundary layer with wall cooling, AFFDL-TR-72-123, Air Force Flight Dynamics Lab., Wright-Patterson Air Force Base, Ohio (1972).
32. L. M. Mack, On the application of linear stability theory to the problem of supersonic boundary-layer transition, AIAA 12th Aerospace Sciences meeting, Washington, D.C. (1974).
33. A. M. O. Smith and H. Gamberoni, Transition, pressure gradient and stability theory, Rept. ES26388, Douglas Aircraft Co. (1956).
34. D. Coles, Measurements of turbulent friction on a smooth flat plate in supersonic flow, *J. Aero. Sci.* **21,** 433 (1954).
35. S. R. Pate and C. J. Schueler, Radiated aerodynamic noise effects on boundary layer transition in supersonic and hypersonic wind tunnels, *AIAA J.* **7,** 450 (1969).
36. Gerlina Keltner, Spatial stability and transition in compressible flat plate flows, Ph.D. Thesis, University of California, Los Angeles (1973).
37. H. B. Squire, On the stability of three-dimensional distribution of viscous fluid between parallel walls, *Proc. R. Soc.* **A142,** 621 (1933).
38. H. Taghavi, Three-dimensional spatial stability and transition of compressible boundary layer flows, Ph.D. Thesis, University of California, Los Angeles (1977).
39. A. R. Wazzan, Spatial stability of Tollmien–Schlichting waves, in *Progress in Aerospace Science* (edited by K. Kuchemann) Vol. 16, p. 99 (1975).

EFFET DU TRANSFERT THERMIQUE SUR LA STABILITE SPATIALE TRIDIMENSIONNELLE ET SUR LA TRANSITION D'UNE COUCHE LIMITE SUR PLAQUE PLANE A MACH 3

Résumé—On étudie la stabilité spatiale linéaire tridimensionnelle des couches limites compressibles sur plaque plane avec transfert thermique dans l'hypothèse de l'écoulement parallèle. L'écoulement moyen est obtenu par les équations classiques de la couche limite avec l'hypothèse de gaz parfait, de viscosité selon la loi de Sutherland et d'un nombre de Prandtl constant.

Des caractéristiques de stabilité, des cartes de stabilité sont obtenues pour des modes bidimensionnels et tridimensionnels à Mach 3 et un rapport de température de paroi par rapport à l'adiabaticité égal à 1,5 ; 1,25 ; 1,0 ; 0,8 ; 0,7 ; et 0,3. Les résultats montrent que la stabilité d'une couche limite ne peut pas être déterminée simplement sur la base du nombre de Reynolds critique. Des calculs pour le premier 3D mode montrent que la variation observée du nombre de Reynolds de transition avec le transfert thermique à la paroi (refroidissement ou chauffage) est prédite qualitativement par la théorie linéaire de l'instabilité. Tandis que la dominance d'un mode d'instabilité peut disparaître lorsque les paramètres principaux affectant la perturbation sont changés, le renversement de la transition est prédit par la théorie linéaire quand le premier mode 3D, qui est stabilisé monotoniquement par le refroidissement cesse d'être important et la transition est alors déterminée par le second mode 2D.

DER EINFLUSS DES WÄRMEÜBERGANGS AUF DIE DREIDIMENSIONALE RÄUMLICHE STABILITÄT UND DEN ÜBERGANG DER GRENZSCHICHT EINER EBENEN PLATTE BEI MACHZAHL 3

Zusammenfassung—Es wird die dreidimensionale lineare räumliche Stabilität kompressibler Grenzschichten an ebenen Platten für den Fall der Parallelströmung untersucht. Den mittleren Strömungszustand erhält man aus den Grundgleichungen kompressibler Grenzschichtströmungen unter der Annahme von Fluideigenschaften wie bei idealen Gasen, der Gültigkeit des Gesetzes von Sutherland für die Viskosität und konstanter Prandtl-Zahl.

Für den zwei- und dreidimensionalen Modus erhält man bei einer Machzahl von 3 Stabilitätscharakteristiken, Verstärkungsverteilungen und Verhältnisse der wirklichen zur adiabaten Wandtemperatur von 1,5 ; 1,25 ; 1,0 ; 0,8 ; 0,7 und 0,3. Die Ergebnisse zeigen, daß die Stabilität einer gegebenen Grenzschichtströmung nicht einfach auf der Grundlage der kritischen Reynolds-Zahl ermittelt werden kann—falsche Schlüsse dürften gezogen werden, wenn nicht die gesamte Instabilitätsverteilung unter besonderer Berücksichtigung von Zuwachsfaktoren in Abhängigkeit von Frequenz und Reynolds-Zahl ausgewertet wird. Berechnungen für den ersten 3D-Modus zeigen, daß mit Ausnahme der "Übergangsumkehrung" die beobachtete Variation der Übergangs-Reynolds-Zahl durch Wärmeübertragung an der Wand (Kühlen und Heizen) qualitativ mit der linearen Instabilitätstheorie beschrieben wird.

Da der vorherrschende Einfluß eines Instabilitätsmodus auf einen anderen übergehen kann, wenn wesentliche die Störung beeinflussende Parameter geändert werden, kann die Übergangsumkehrung auch durch die lineare Theorie beschrieben werden, wenn bei Kühlung mittels vegrößerter Oberfläche der erste 3D-Modus, der durch Kühlung monoton stabilisiert wird, an Bedeutung verliert und der Übergang dann durch den zweiten 2D-Modus bestimmt wird.

ВЛИЯНИЕ ТЕПЛОПЕРЕНОСА НА ТРЕХМЕРНУЮ ПРОСТРАНСТВЕННУЮ УСТОЙЧИВОСТЬ И ПЕРЕХОД ПОГРАНИЧНОГО СЛОЯ НА ПЛОСКОЙ ПЛАСТИНЕ ПРИ $Ma = 3$

Аннотация—Исследуется трехмерная линейная пространственная устойчивость сжимаемых пограничных слоев на плоской пластине в предположении параллельности потока. Среднее течение определяется из стандартных уравнений сжимаемого пограничного слоя в предположении идеальности свойств газа, закона вязкости Сэзерленда и постоянного числа Прандтля.

Получены кривые устойчивости для двухмерных и трехмерных течений при $Ma = 3$ и отношениях температуры стенки к ее адиабатической температуре, равных 1,5 ; 1,25 ; 1,0 ; 0,8 ; 0,7 и 0,3. Результаты показывают, что устойчивость рассматриваемого пограничного слоя нельзя определять только по критическому числу Рейнольдса можно придти к неправильным выводам, если не будет рассчитана вся диаграмма неустойчивости, особенно зависимость коэффициентов усиления от частоты и числа Рейнольдса. Расчеты, выполненные для первой трехмерной структуры течения, показывают, что за исключением "переходной области возвратного течения" наблюдаемое изменение переходного числа Рейнольдса с изменением теплопереноса на стенке (охлаждение и нагрев) можно рассчитать качественно с помощью линейной теории устойчивости. Кроме того, поскольку основная мода неустойчивости может изменяться с изменением основных, влияющих на возмущение, параметров, рециркуляционные зоны можно рассчитать по линейной теории в том случае, когда при охлаждении поверхности первая трехмерная структура течения, монотонно стабилизирующаяся при охлаждении, перестает играть доминирующую роль, и переходный процесс определяется тогда второй двухмерной структурой.